https://doi.org/10.1038/s44304-026-00196-6

Assessment of ground-motion prediction equations using observations and information theory: application to the Northeastern Tibetan Plateau

Youtian Yang[1,2] ✉, Alik Ismail-Zadeh[1] & Jidong Wu[3,4]

Ground-motion prediction equations (GMPEs) are fundamental to seismic hazard assessment, yet their applicability is difficult to evaluate in tectonically complex regions where instrumental observations are sparse or absent, such as the northeastern Tibetan Plateau. We evaluate representative GMPEs using two approaches: residual-based error metrics and an information-theory-based evaluation. The two recent earthquakes, the 2022 Menyuan and 2023 Jishishan events, provide an opportunity to examine model behavior under observed conditions. The information-theory-based approach is first applied to these two earthquakes to verify feasibility and to compare with residual-based outcomes, and is then extended to two large historical earthquakes in the region, the 1920 Haiyuan earthquake and the 1927 Gulang earthquake, to assess stability under extrapolative, data-limited conditions. Across these applications, the information-theory-based evaluation yields consistent rankings and stable weights, whereas the residual analysis captures event-specific variability. Together, the two approaches provide complementary insight into model applicability and offer a practical basis for ground-motion assessment and extrapolation in tectonically complex and observationally sparse regions.

The northeastern margin of the Tibetan Plateau (NETP) represents a tectonically intricate and seismically active segment of the India–Eurasia collision zone[1,2]. This region exhibits a complex interplay of crustal shortening, lateral extrusion, and active faulting, resulting in diverse rupture styles and persistent seismic activity, and it has experienced frequent large-magnitude earthquakes throughout historical and geological times[3–5]. The NETP is situated (Fig. 1) at the junction of the Qilian Orogen, the East Kunlun Orogen, the Alxa Block, the Ordos Block, and the western segment of the Qinling Orogen[6–8]. This region is one of the most intensely deformed areas within the Late Cenozoic tectonic zone characterized by a dense distribution of active faults. The strong interactions and tectonic transformations among these faults play a critical role in generating tectonic stresses and large earthquake occurrences in the region[9–16].

The study region (Fig. 1) experienced 43 earthquakes of magnitude 6 and greater, including 1920 Haiyuan Mw 8.2 earthquake, one of the strongest events in mainland China[17]. Moreover, studies based on geodetic (GPS) measurements and numerical modeling suggest a high potential for future large-magnitude seismic activity in the region[5,8,18,19].

Due to the complex geodynamic setting and significant seismic potential of the NETP, several major infrastructure systems in the region face considerable risk. A prominent example is the Longyangxia-Qingtongxia hydropower cascade, which contributes over 15% of China's total hydroelectric generation and extends along the river from approximately 36°N, 101°E to 38°N, 106°E. The seismic hazard and vulnerability/exposure of critical infrastructure in this area highlight the need for accurate ground-motion modeling to support seismic risk assessment and disaster management strategies.

A Ground-Motion Prediction Equation (GMPE) describes the relationship between ground-motion parameters, such as peak ground acceleration (PGA), peak ground velocity (PGV) or spectral acceleration (SA); the characteristics of an earthquake, including its magnitude, source-to-site distance, rupture distance, and fault type; and site conditions, represented by

[1]Institute of Applied Geosciences, Karlsruhe Institute of Technology, Karlsruhe, Germany. [2]School of System Science, Beijing Normal University, Beijing, China. [3]School of National Safety and Emergency Management, Beijing Normal University, Beijing, China. [4]Joint International Research Laboratory of Catastrophe Simulation and Systemic Risk Governance, Beijing Normal University at Zhuhai, Zhuhai, China. ✉e-mail: yangyoutian@mail.bnu.edu.cn

soil type or S-wave seismic velocity within the upper 30 m (Vs30). GMPEs are widely used in seismic hazard analysis and earthquake impact prediction[20,21], and they are typically specific to particular regions and tectonic settings. Nevertheless, global GMPE models such as the Next Generation Attenuation (NGA) relations may exhibit systematic biases when applied to specific localities[22–25], motivating the development of regional models, e.g., for the Himalaya region[26]. Currently, no targeted or systematic validation of GMPEs exists for the NETP region[27,28], raising concerns about the reliability of existing models for simulating and predicting ground motions. Moreover, strong-motion records in the region are extremely limited; only the 2022 Menyuan and 2023 Jishishan earthquakes (Fig. 1) provide instrumental ground-motion datasets. As a result, the development of new GMPEs based solely on local observations is constrained. A more practical and effective approach is to identify and select existing models that are better suited to the NETP region.

There are two commonly used approaches for evaluating the performance of GMPEs. The first relies on statistical metrics, such as root-mean-square error (RMSE) and mean absolute error (MAE), which quantify discrepancies between observed and predicted ground motions. This method is effective; however, its applicability is highly dependent on the availability and quality of observational data. The second approach, based on information theory, provides a robust alternative for assessing ground-motion prediction models, particularly in data-sparse environments or when observational records are incomplete or unreliable[29]. Unlike residual-based methods that require direct comparisons with recorded data, this approach quantifies the relative information loss between model predictions and observed distributions[30]. In addition, it helps identify models with better overall predictive capability and enables the derivation of normalized weights based on divergence metrics. These weights can be used to construct composite ground-motion models through probabilistic integration, offering a flexible and theoretically grounded means of accounting for model uncertainty[31,32].

To address these challenges, this study develops a framework that combines residual-based metrics with information-theory-based criteria to assess the applicability of five representative GMPEs in the northeastern Tibetan Plateau. The residual-based evaluation focuses on two recent earthquakes, the 2022 Menyuan strike-slip event and the 2023 Jishishan thrust event, where observations allow direct assessments of the model performance. The information-theory-based approach is first applied to these same two earthquakes to verify its feasibility and consistency with observation-based analyses, and is then extended to the 1920 Haiyuan and 1927 Gulang earthquakes to evaluate model stability under extrapolative, data-limited conditions. Through this two-stage evaluation, the study aims to bridge observation-based and extrapolative assessments, demonstrating how residual analysis and information-theory-based weighting provide complementary perspectives on GMPE performance.

Results

Residual-based GMPEs evaluation

The Menyuan earthquake (Mw 6.6, Ms 6.9) occurred on January 8, 2022, with a hypocentral depth of 10 km and an epicenter at 37.77°N, 101.25°E (China Earthquake Networks Center, http://www.ceic.ac.cn). It was identified as a strike-slip event[19]. For the Menyuan Earthquake, the predicted PGA values from five GMPEs and observed PGA are shown in Fig. 2. The five GMPEs exhibit distinct predictive behaviors. Huo and Hu[33] model (Fig. 2a) generally follows the one-to-one line but tends to overestimate at larger PGA levels. Si and Midorikawa[34] model (Fig. 2b) displays a relatively wide vertical scatter around the reference line, indicating greater variability, though without clear systematic bias. GB[35] model (Fig. 2c) provides a more balanced fit, with predictions closely aligned with the observations across the full range. Zhou[36] model (Fig. 2d) consistently overestimates PGA, with most points falling above the one-to-one line. Wang[28] model (Fig. 2e) shows the most stable performance, characterized by tightly clustered data points around the reference line and the smallest residual dispersion. Despite these differences, all models capture the overall relationship between predicted and observed PGAs.

Table 1 and Fig. 2 illustrate the relative performance of the five GMPEs. Wang[28] model stands out, exhibiting the lowest RMSE, MAE, and BIAS values, as well as the highest overall consistency with observations. In contrast, Zhou[36] model shows the largest errors across all three metrics and the weakest agreement with the recorded data. Huo and Hu[33], Si and Midorikawa[34], and GB[35] fall in an intermediate range: Huo and Hu yields lower overall errors but exhibits a larger bias; Si and Midorikawa presents more balanced metric values despite larger scatter; and GB[35] shows relatively higher errors and weaker consistency compared with the other two.

The Mw 6.2 (Ms 6.5) Jishishan earthquake occurred on December 19, 2023, with a hypocentral depth of 10 km and an epicenter at 35.70°N, 102.79°E (China Earthquake Networks Center, http://www.ceic.ac.cn). It was classified as a thrust fault event[37]. For the Jishishan earthquake, as shown in Fig. 3a, the Huo and Hu[33] predictions broadly follow the one-to-one line with moderate scatter, although underestimation becomes evident at larger PGA levels. Si and Midorikawa[34] (Fig. 3b) exhibits greater variability than Huo and Hu[33], with a wider vertical spread and more pronounced deviations at strong shaking levels. GB[35] (Fig. 3c) yields relatively compact results, but its bias varies with shaking intensity, tending to overestimate weak motions and underestimate strong ones. Zhou[36] (Fig. 3d) shows the largest dispersion among the first four models, particularly at higher PGA values. Wang[28] (Fig. 3e) displays the widest overall scatter, with systematic departures from the one-to-one reference line becoming more apparent at the upper end of the PGA range. Overall, all models show a consistent trend of overestimating low PGA values and underestimating high ones.

The quantitative comparison provided by the radar plot (Fig. 3f) and Table 1 highlights clear differences in model performance. Huo and Hu[33] exhibits moderate error levels and bias, with an R^2 value higher than that of Si and Midorikawa[34] but lower than GB[35]. Si and Midorikawa[34] performs similarly to Huo and Hu[33], though with slightly larger errors and weaker correlation. GB[35] stands out among the five models, showing the lowest RMSE and MAE and the highest R^2, indicating the best consistency with the observations. Zhou[36] yields the second-largest errors, reflecting reduced predictive reliability. Wang[28] shows the highest RMSE, MAE, and BIAS and the lowest R^2, making it the weakest model in this comparison. All five models exhibit negative BIAS values, indicating that they systematically underestimated GMs during the Jishishan earthquake.

For the cross-event overall model ranking across the Menyuan and Jishishan earthquakes, Table 2 summarizes the results of the relative scoring method (Eqs. 6–8) for both events, together with the aggregated cross-event performance. For each earthquake, the *total score* represents the sum of the individual record-level scores, while the *average score* is the mean score across all records for that event. Because the two earthquakes differ substantially in the number of GM records, the overall model performance is measured using the cross-event average score, obtained by averaging the two event-specific average scores. In addition, the *combined rank* is calculated as the sum of the event-level rankings, providing an equally weighted indicator of cross-event consistency.

The scoring results are consistent with the residual-based analysis shown in Table 1. For the Menyuan earthquake, Wang[28] ranks first with the highest total score, followed by GB[35], Si and Midorikawa[34], and Huo and Hu[33] in descending order, while Zhou[36] yields the lowest score and ranking, reflecting large prediction errors and systematic bias. For the Jishishan earthquake, GB[35] obtains the highest total score and ranks first, with Huo and Hu[33] and Si and Midorikawa[34] showing intermediate performance, and Zhou[36] and Wang[28] ranking fourth and fifth, respectively, indicating limited predictive capability for this event.

Overall, considering both earthquakes together, GB[35] attains the highest cross-event average score and the lowest combined rank, indicating the most stable and accurate predictive performance across the two events. Huo and Hu[33] and Si and Midorikawa[34] exhibit moderate performance for both earthquakes, with Huo and Hu showing a slightly higher cross-event average score than Si and Midorikawa. Wang[28] performs well for the Menyuan earthquake, but its predictive accuracy decreases substantially for the Jishishan earthquake, resulting in a mid-range overall ranking. Zhou[36]

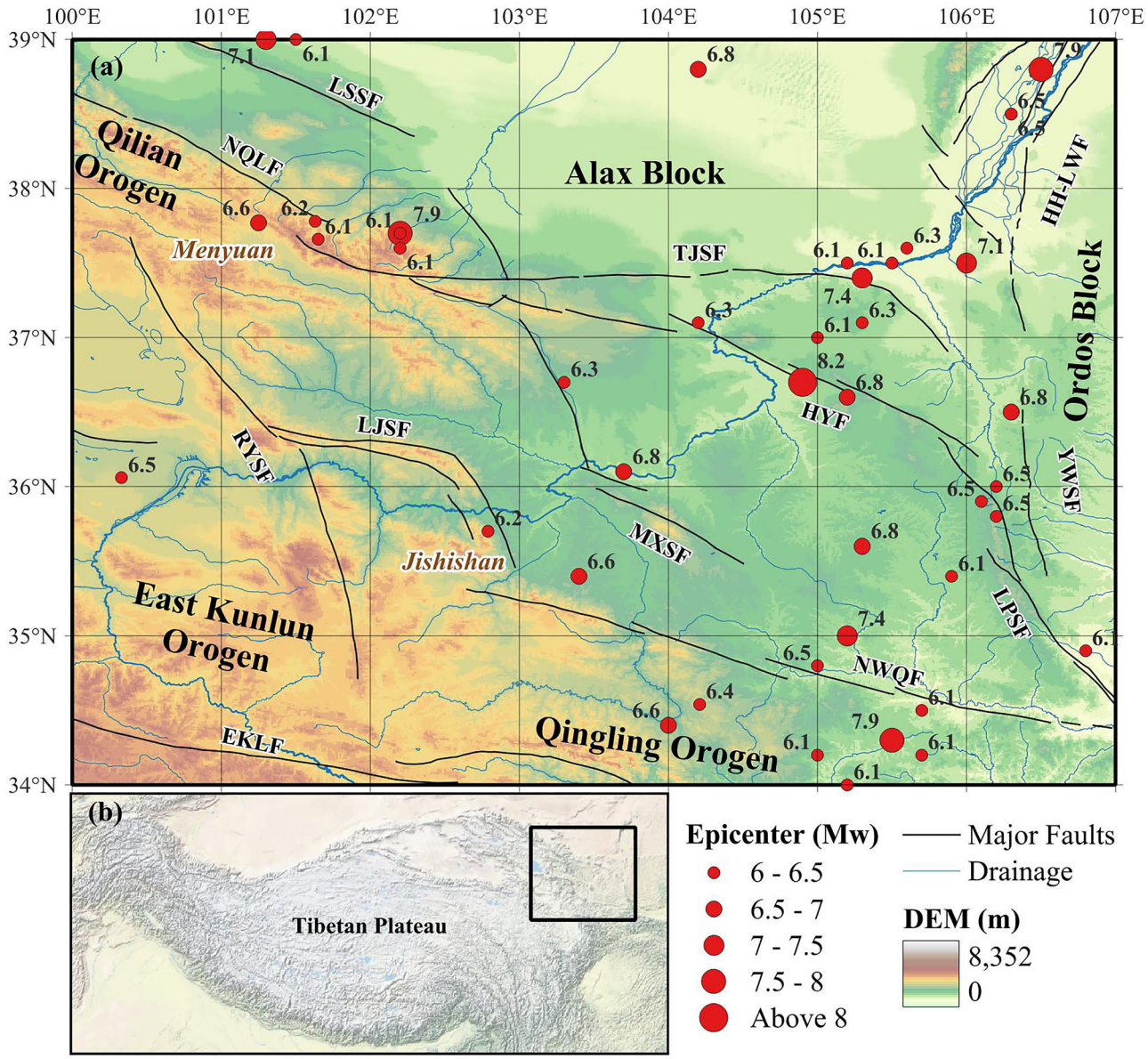

Fig. 1 | Overview of the study area. a Map of the study area showing the geological structure, major faults (black lines), and earthquakes (red circles) with moment magnitudes Mw ≥ 6 since 1000 AD. Earthquake data are presented in the Supplementary Information. LSSF Longshoushan Fault, NQLF North Qilian Fault, RYSF Riyueshan Fault, LJSF Laijshan Fault, EKLF East Kunlun Fault, NWQF northern margin of the West Qingling Fault, LPSF Liupanshan Fault, YWSF Yunwushan Fault, MXSF Maxianshan Fault, HYF Haiyuan Fault, TJSF TIanjingshan Fault, HH-LWF Huanghe-Lingwu Fault. **b** Location of the study area (black box) relative to the Tibetan Plateau. Topography derived from SRTM digital elevation model.

shows poor overall performance due to large and persistent prediction errors.

Information-theory-based GMPEs evaluation. While the residual-based evaluation provides direct insights into the predictive accuracy of each GMPE, it is inherently sensitive to the quantity and quality of available ground-motion records. In regions such as the northeastern Tibetan Plateau, where strong-motion data are sparse and unevenly distributed, this limitation may affect the reliability of model comparisons. To address this issue and to assess the robustness of the models under varying data conditions, an information-theory-based framework was further applied.

This approach evaluates model performance based on statistics derived from GMPE model outputs, making it applicable to earthquakes in the absence of observations. In this study, two recent events—the 2022 Menyuan and 2023 Jishishan earthquakes—and two large historical events—the 1920 Haiyuan and 1927 Gulang earthquakes – were analyzed. The recent earthquakes enable direct comparison with the residual-based results, whereas the historical events provide an opportunity to examine model stability and extrapolation capability under limited data constraints.

A distance threshold of 500 km was adopted to define the calculation range for the 2022 Menyuan and 2023 Jishishan earthquakes, and 700 km for the 1920 Haiyuan and 1927 Gulang earthquakes. The selection of a reasonable distance threshold and its influence on the evaluation results are discussed in Section S3 of the *Supplementary Information*.

For Instrumental earthquakes, the 2022 Menyuan and 2023 Jishishan earthquakes are summarized in Table 3. For the Menyuan earthquake, Wang[28] achieves the highest weight (0.386), followed by Huo and Hu[33] and GB[35], whereas Si and Midorikawa[34] and Zhou[36] show negative DSI values and are therefore excluded from further consideration. For the Jishishan earthquake, Wang[28] again ranks first (0.375), followed by Huo and Hu[33] and

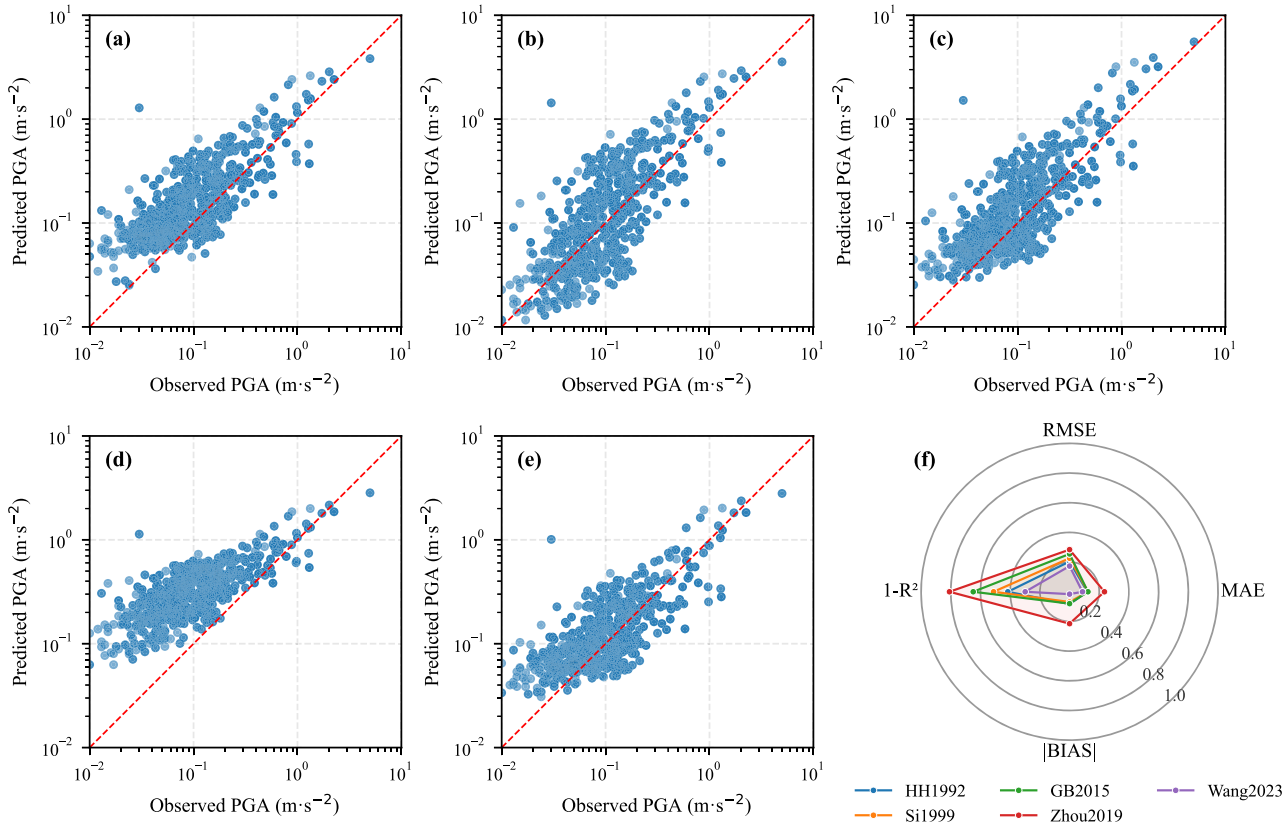

Fig. 2 | Comparison of observed and predicted PGAs for the Menyuan earthquake using five GMPEs. a Huo and Hu[33], **b** Si and Midorikawa[34], **c** GB[35], **d** Zhou[36], and **e** Wang[28] models. Here and in Fig. 3, **a**–**e** are scatter plots of observed versus predicted PGA, where blue dots represent GM values. All plots use logarithmic scales for both axes, and the red dashed line denotes the one-to-one reference line. **f** Presents a radar chart summarizing residual-based evaluation metrics: RMSE, MAE, BIAS (absolute value), and $1 - R^2$. Here and in Fig. 5, values closer to the origin indicate better performance.

Table 1 | Residual-based evaluation metrics for the Menyuan and the Jishishan earthquake

Earthquake		Huo and Hu[33]	Sin and Midorikawa[34]	GB[35]	Zhou[36]	Wang[28]
Menyuan	*RMSE*	0.204	0.226	0.255	0.284	0.173
	MAE	0.12	0.124	0.124	0.235	0.087
	BIAS	0.083	0.069	0.08	0.215	0.016
	R^2	0.584	0.488	0.351	0.191	0.701
Jishishan	*RMSE*	0.735	0.782	0.623	0.847	0.882
	MAE	0.286	0.302	0.255	0.325	0.357
	BIAS	−0.25	−0.283	−0.212	−0.251	−0.35
	R^2	0.43	0.354	0.59	0.244	0.179

GB[35]. Compared with the Menyuan event, the weight differences among the selected models are smaller for Jishishan, with Huo and Hu[33] and GB[35] exhibiting nearly identical weights.

Although the rankings derived from the information-theory-based evaluation differ from those obtained through the residual-based analysis (Table 2), the two approaches show partial consistency in identifying models with relatively good predictive capability. For the Menyuan earthquake, Wang[28] ranks first in both methods, while GB[35], which performed well in the residual-based analysis, was also selected in the information-theory-based evaluation. For the Jishishan earthquake, both approaches consistently identify GB[35] and Huo and Hu[33] as reliable models. This consistency suggests that, despite methodological differences, the information-theory-based approach can identify models that remain reliable even under limited or uneven data conditions, supporting its applicability to multiple events and data-sparse regions.

The relatively high information-theory-based scores obtained by models that ranked lower in the residual-based analysis, such as Si and Midorikawa[34] for the Menyuan earthquake and Wang[28] for the Jishishan earthquake, may be partly explained by the different evaluation logic between the two frameworks. The residual-based method emphasizes absolute deviations from observations, whereas the information-theory-based framework evaluates relative consistency among all models.

For historical earthquakes, two largest earthquakes that have occurred in the NETP region since 1900 were selected. The 1920 Haiyuan Mw 8.1 (Ms 8.5) strike-slip earthquake, with an epicenter around 105.3° E, 36.6° N and a focal depth of 17 km, and the 1927 Gulang Mw 7.7 (Ms 7.9) thrust-dominated earthquake, with an epicenter near 102.6° E, 37.6° N and a focal depth of 15 km. These two events represent the largest-magnitude earthquakes to have struck the region over the past century and thus provide critical references for regional seismic hazard assessment. Details of

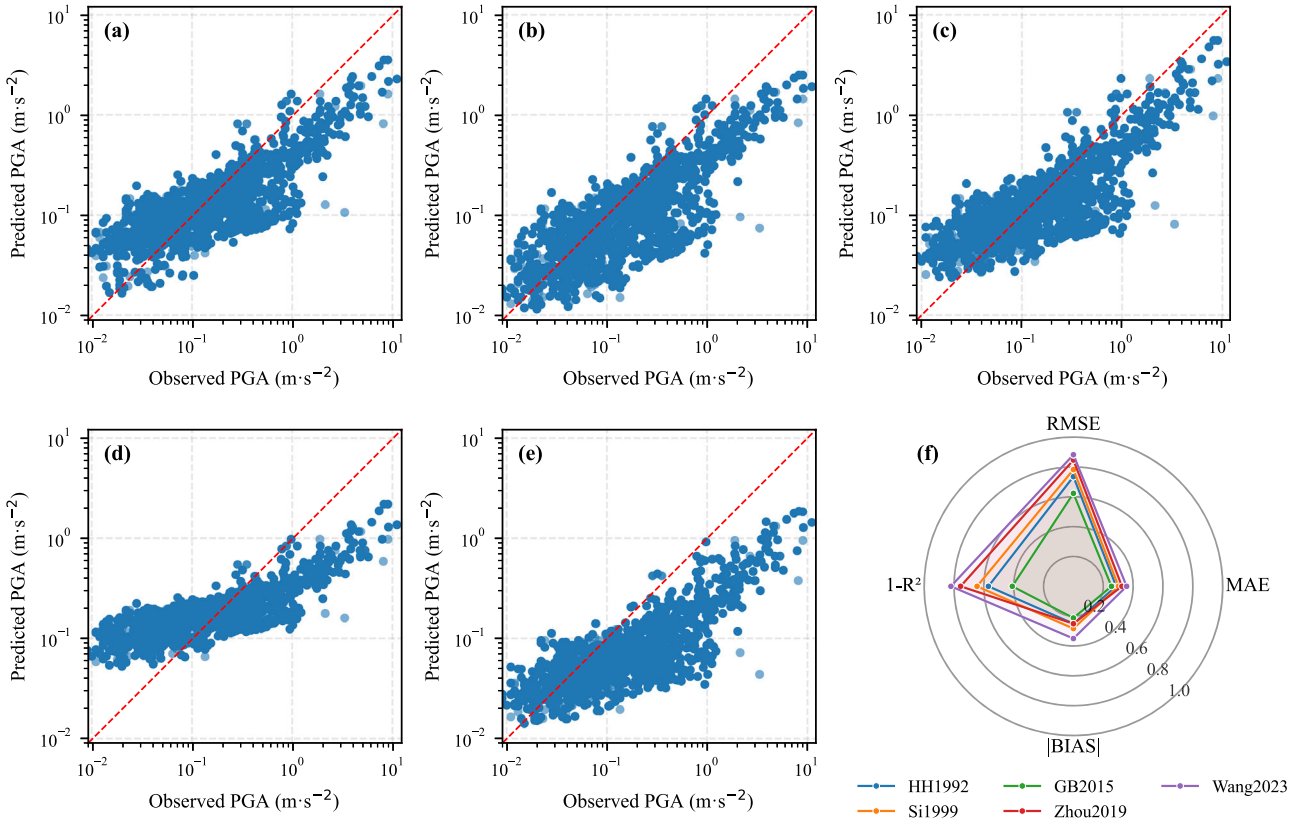

Fig. 3 | Comparison of observed and predicted PGA for the Jishishan earthquake using five GMPEs. See Fig. 2 for description of panels.

Table 2 | Residual-based scores and rankings for the Menyuan and Jishishan earthquake

Earthquake		Huo and Hu[33]	Si and Midorikawa[34]	GB[35]	Zhou[36]	Wang[28]
Menyuan	Total score	4099	4312	4789	2328	5122
	Average score	3.474	3.546	4.058	1.973	4.341
	Rank	4	3	2	5	1
Jishishan	Total score	56,487.5	50445.5	58,843.5	46,814.5	39,531.5
	Average score	3.921	3.501	4.084	3.249	2.744
	Rank	2	3	1	4	5
Overall	Average score	3.698	3.524	4.071	2.611	3.543
	Combined rank	6	6	3	9	6

magnitude, epicentral location, and focal depth are provided in the Supplementary Information.

Table 4 presents the information-theory-based evaluation results for the 1920 Haiyuan and 1927 Gulang earthquakes. For both events, Wang[28] achieves the highest likelihood and weight, ranking first, whereas Huo and Hu[33] ranks second, offering meaningful but comparatively smaller weight, and GB[35] ranks third with a modest contribution. In contrast, Si and Midorikawa[34] and Zhou41 produce negative weights and are excluded from the model combination. The consistent ranking across these two earthquakes indicates that the relative applicability of these GMPEs remains stable in the NETP region, with Wang[28] serving as the dominant model and Huo and Hu[33] and GB[35] providing supplementary contributions.

The strong agreement between the Haiyuan and Gulang results demonstrates the robustness of the information-theory-based approach in scenarios where observational data are limited or unevenly distributed. This stability contrasts with the variability often observed in residual-based analyses, where model rankings may shift between events due to differences in faulting mechanisms or record availability. Therefore, the information-theory-based method provides a complementary perspective, providing a statistically grounded means of assessing cross-event consistency and deriving stable model weights for regional seismic hazard evaluation.

Discussion

The residual-based and information-theory-based evaluations provide complementary perspectives on GMPE applicability in the NETP, revealing both event-specific performance variability and stable cross-event model behavior. Residual analyses demonstrate that predictive accuracy differs markedly between earthquakes, whereas the information-theory-based framework identifies consistent model rankings across multiple events, including historical earthquakes lacking instrumental observations. Together, these results provide a coherent basis for model evaluation under conditions of limited data and complex tectonic environments.

Residual analysis highlights a pronounced contrast between the Menyuan and Jishishan earthquakes. While all evaluated GMPEs perform reasonably well for the Menyuan strike-slip event, predictive accuracy declines substantially for the Jishishan thrust earthquake. Differences in source mechanism provide a possible explanation. Thrust earthquakes commonly generate higher stress drops and stronger near-field motions

Table 3 | Information-theory-based evaluation for the Menyuan and Jishishan earthquakes

Earthquake	Model	LLH	DSI	Weight	Rank
Menyuan	Huo and Hu[33]	1.662	10.560	0.322	2
	Si and Midorikawa[34]	2.383	−32.898	−1.000	--
	GB[35]	1.802	0.362	0.292	3
	Zhou[36]	1.971	−10.695	−1.000	--
	Wang[28]	1.399	32.672	0.386	1
Jishishan	Huo and Hu[33]	1.801	6.328	0.316	2
	Si and Midorikawa[34]	2.394	−29.512	−1.000	--
	GB[35]	1.834	3.941	0.309	3
	Zhou[36]	1.993	−6.935	−1.000	--
	Wang[28]	1.554	26.178	0.375	1

Table 4 | Information-theory-based evaluation for the Haiyuan and Gulang earthquakes

Earthquake	Model	LLH	DSI	Weight	Rank
Haiyuan	Huo and Hu[33]	1.476	26.542	0.316	2
	Si and Midorikawa[34]	2.654	−44.065	−1.000	--
	GB[35]	1.759	4.047	0.260	3
	Zhou[36]	2.993	−55.782	−1.000	--
	Wang[28]	1.057	69.258	0.423	1
Gulang	Huo and Hu[33]	1.594	23.070	0.311	2
	Si and Midorikawa[34]	2.680	−42.051	−1.000	--
	GB[35]	1.801	6.619	0.269	3
	Zhou[36]	3.010	−53.887	−1.000	--
	Wang28	1.160	66.249	0.420	1

than strike-slip events[38], resulting in more complex shaking patterns that are more difficult to capture with empirical models. The Jishishan earthquake also exhibited unilateral rupture and strong directivity, producing asymmetric ground-motion distribution and enhanced PGA toward the northwest of the epicenter[37]. Regional site conditions likely further contributed to the degraded predictive performance. Compared with Menyuan, the Jishishan region is closer to the Loess Plateau and is characterized by thicker Quaternary loess deposits, which are known to amplify seismic waves[39]. Lower Vs30 values around the Jishishan epicenter support the presence of softer near-surface materials, suggesting that combined effects of rupture complexity, directivity, and site amplification jointly contribute to the observed model–data discrepancies.

Whereas residual analysis emphasizes event-specific performance, the information-theory-based evaluation provides a complementary cross-event perspective. By comparing statistical characteristics of predicted ground-motion distributions rather than relying solely on observation-based residuals, this framework reduces sensitivity to data sparsity and enables comparison across earthquakes with heterogeneous data availability. Importantly, it also assigns normalized weights to each GMPE, allowing models to be combined according to their relative applicability rather than selecting a single "best" model. Across four representative earthquakes, the 2022 Menyuan, 2023 Jishishan, 1920 Haiyuan, and 1927 Gulang events, Wang[28], Huo and Hu[33], and GB[35] are repeatedly identified as the most representative models. The persistence of these rankings across independent events, including historical earthquakes without instrumental records, indicates stable cross-event applicability that is not fully captured by residual-based comparisons alone.

Several uncertainties and limitations should be acknowledged. Part of the uncertainty arises from data-related aspects, including earthquake source parameters and site characteristics. For the 2022 Menyuan and 2023 Jishishan earthquakes, we use epicentral location, focal depth, magnitude, and observed GM data. All these data are derived from instrumental observations and are considered relatively reliable. For the 1920 Haiyuan and 1927 Gulang earthquakes, the epicentral location, focal depth, and magnitude are associated with uncertainties due to their historical nature. Such uncertainties may affect the absolute PGA values predicted by the five GMPEs. However, the information-theory-based evaluation is conducted under identical parameter conditions for each event, and these uncertainties are not dominant in the evaluation. An analysis of earthquake parameter uncertainties for these two earthquakes is provided in the Supplementary Information. In addition, only two earthquakes provide sufficiently dense instrumental coverage, so any mechanism-related tendencies, such as the apparent preference of Wang[28] for strike-slip events and GB[35] for thrust events, should be considered suggestive rather than definitive. The Vs30 data used in this study are derived from a global model constructed using topographic-slope proxies, which may not fully capture local site conditions compared with site-specific Vs30 measurements. Given the pronounced influence of loess deposits on ground-motion amplification in the study region, the incorporation of more detailed site-condition parameters represents an important direction for future studies.

From a methodological perspective, differences in the functional forms of GMPEs imply that source, path, and site effects are represented in different ways. These formulation differences lead to differences in model performance when earthquakes with different mechanisms and geological settings are compared. The information-theory-based approach assumes that GM data follow a normal distribution. Therefore, the functional form of a GMPE may influence the evaluation results. In addition, the spatial extent of ground-motion sampling, defined by the selected distance threshold from the earthquake epicenter, directly influences the sample size and its statistical distribution, thereby affecting the evaluation results. Details regarding the distance threshold analysis are provided in the Supplementary Information. These uncertainties highlight the need for continued refinement of regional site characterization, further accumulation of high-quality strong-motion data, and broader validation across additional earthquakes to improve the robustness of GMPE applicability assessments in the NETP region.

In summary, this study underscores the value of incorporating observational and information-theoretic perspectives in GMPE evaluations. The dual-framework facilitates more robust model selection and allows for the derivation of normalized weights that reflect relative applicability across diverse scenarios. This framework enhances confidence in GMPE selection and provides a practical basis for ground-motion estimation in tectonically complex and observationally data-limited regions such as the NETP region. Future work should incorporate additional well-recorded earthquakes, refine regional site characterization through improved Vs30 constraints, and examine the transferability of this framework to other earthquake-prone regions.

Methods

Strong ground motion observation

This study utilizes ground motion (GM) recordings from the 2022 Menyuan and the 2023 Jishishan earthquakes. As shown in Fig. 4, a total of 1180 surface PGA values were obtained for the Menyuan earthquake, whereas the Jishishan event yielded 14,407 surface strong-motion records due to denser instrumentation and more favorable station coverage at the time of occurrence[40].

The highest recorded PGA for the Menyuan earthquake was 4.99 m s^{-2}. Although the Jishishan earthquake had a lower magnitude, it generated significantly higher PGA values, reaching up to 11.08 m s^{-2}. The relatively strong ground motions observed during the Jishishan event are attributed to multiple factors, including its thrust-fault focal mechanism and substantial site amplification effects associated with loess deposits[37,41]. Although these are currently the only two strong-motion datasets available within the study region, their differences in source mechanism and site

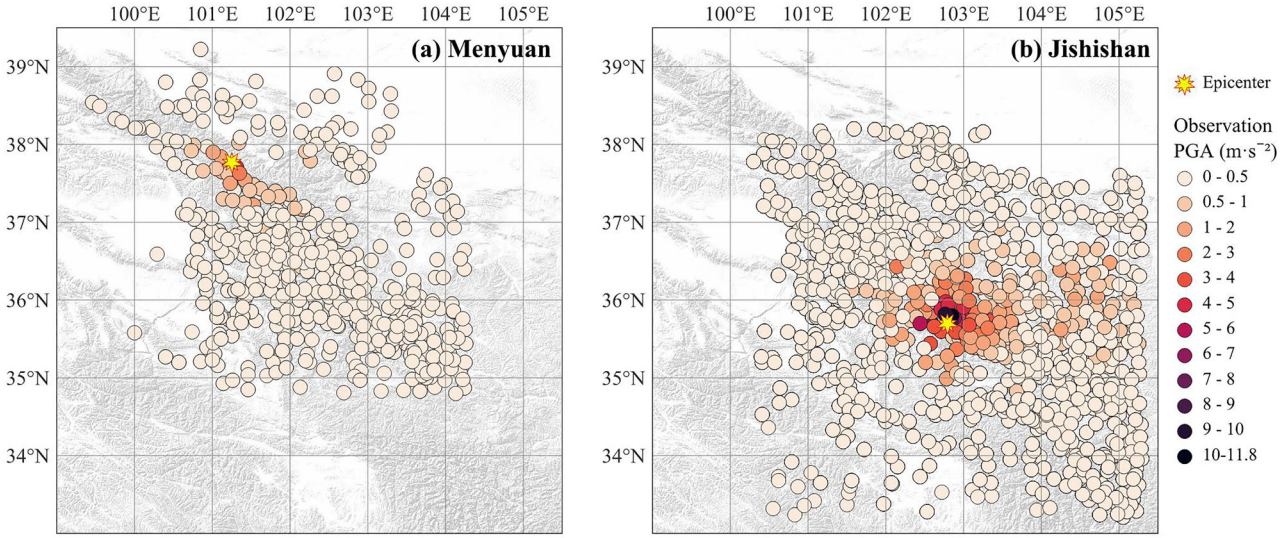

Fig. 4 | Distribution of PGA values (colored circles) recorded by strong-motion stations. a The 2022 Menyuan earthquake and **b** The 2023 Jishishan earthquake. Background hillshade derived from SRTM digital elevation model.

conditions provide a valuable basis for evaluating GMPE performance under varying seismic scenarios.

Vs30 data

Information on site conditions was incorporated into the strong-motion dataset using Vs30, obtained from the United States Geological Survey (USGS) global Vs30 model (https://earthquake.usgs.gov/data/vs30/) at spatial resolution of 30 arc-s (~1 km). This dataset provides a consistent and widely used reference for site classification and characterization in regions lacking detailed local measurements. The spatial distribution of Vs30 in the study area is shown in Fig. 5. Throughout this paper, "Vs30" refers specifically to the values derived from this dataset.

Selected GMPEs for the NETP

Considering that PGA is commonly used to represent seismic hazard in engineering safety evaluations and risk assessments, this study selects PGA as the target ground-motion parameter in the GMPE models. To identify GMPEs suitable for the NETP, a preliminary selection was conducted based on the following criteria: a model was chosen if it (a) was developed using strong-motion data from the NETP, either entirely or partially; (b) was specifically adjusted or optimized for earthquakes in the NETP; or (c) had been applied to NETP earthquakes and demonstrated applicability through validation. Based on these criteria, five GMPEs were selected for this study: Huo and Hu[33], Si[34], GB[35], Zhou[36], and Wang[28].

Detailed information on each model is provided below. In the following, R_e denotes the distance (km) from the earthquake epicenter to the selected site; R_h denotes the distance (km) from the earthquake hypocenter to the selected site; and D represents the focal depth (m).

(a) Huo and Hu[33]:

$$\log_{10}\mathrm{PGA} = C_1 + C_2\mathrm{M_s} + C_3\mathrm{M_s^2} + C_4\log_{10}\left(\mathrm{R_h} + C_5 * \exp\left(\mathrm{C_6M_s}\right)\right),$$
$$\begin{cases} C_1 = -1.822, C_2 = 1.448, C_3 = -0.052, C_4 = -2.018, C_5 = 0.1818, C_6 = 0.7072, \text{forrock}, \\ C_1 = -1.164, C_2 = 1.203, C_3 = -0.044, C_4 = -1.650, C_5 = 0.1818, C_6 = 0.7072, \text{forsoil}. \end{cases} \quad (1)$$

Huo and Hu[33] model is an early GMPE developed for China based on the conversion of intensity data[42] and has remained widely used, including the NETP region[43,44]. Rock sites are defined as Vs30 > 760 m s$-$, and soil sites as Vs30 ≤ 760 m s$-$. For each computational grid cell, the site is first classified as rock or soil based on its Vs30 value (Fig. 5), and the predicted PGA is then computed using Eq. (1).

(b) Si and Midorikawa[34]:

$$\log_{10}\mathrm{PGA} = 0.5M_w + C_1D - \log_{10}\left(R_e + C_2 * 10^{0.5M_w}\right) - C_3R_e + C_4$$
$$C_1 = 0.0043, C_2 = 0.0055, C_3 = 0.003, C_4 = 0.61 \quad (2)$$

Si and Midorikawa[34] model has proven effective for the post-earthquake rapid evaluations[45] and seismic hazard assessments within the region[46,47]. It was originally developed for soil sites, defined as locations with Vs30 < 1140 m s^{-1} [35].

(c) GB[35]:

$$\log_{10}\mathrm{PGA} = C_1 + C_2M_s + C_3\log_{10}\left(R_e + C_4 * \exp(C_5M_s)\right)$$
$$\begin{cases} C_1 = 0.561, C_2 = 0.746, C_3 = -1.925, C_4 = 0.956, C_5 = 0.462, \text{if} M_s \le 6.5 \\ C_1 = 2.501, C_2 = 0.448, C_3 = -1.925, C_4 = 0.956, C_5 = 0.462, \text{if} M_s \ge 6.5 \end{cases} \quad (3)$$

GB[35] model was developed for the current seismic zoning map of China[27]. Equation (3) applies to medium-dense soil site, while predictions for other site classes are obtained by adjusting this reference using site amplification factors; the detailed procedure is provided in the *Supplementary Information*.

(d) Zhou[36]:

$$\log_{10}\mathrm{PGA} = C_1 + C_2M_w + C_3M_w^2 + C_4 * \log_{10}\left(R_e + C_5 * \exp(C_6M_w)\right) + C_7{R_e}^2 + C_8R_e$$
$$C_1 = -1.26102, C_2 = 1.203, C_3 = -0.044, C_4 = -1.65, C_5 = 0.1818$$
$$C_6 = 0.7072, C_7 = -9.82429 * 10^{-6}, C_8 = 0.0050472 \quad (4)$$

for soil.

This model is based on Huo and Hu[33], with soil-site adjustments targeted to western China (including the NETP); for rock sites, the Huo and Hu model is retained (Eq. 1).

(e) Wang[28]:

$$\ln\mathrm{PGA} = C_1 + C_2M_w + C_3\left(8.5 - M_w\right)^2 + \left(C_4 + C_5M_w\right)\ln\left(\sqrt{\mathrm{R_h}^2 + C_6^2}\right) + C_7\ln\left(\frac{V_{s30}}{760}\right)$$
$$+C_8\exp(C_9(V_{s30} - 360))\ln\left(\frac{\mathrm{PGA_r} + C_{10}}{C_{10}}\right) + \mathrm{f_{hng}} + \mathrm{f_{flt}}$$
$$C_1 = 8.8987, C_2 = -0.8896, C_3 = -0.2112, C_4 = -3.0899, C_5 = 0.2673,$$
$$C_6 = 10.3706, C_7 = -0.568, C_8 = -0.1720, C_9 = -0.0067, C_{10} = 0.1 \quad (5)$$

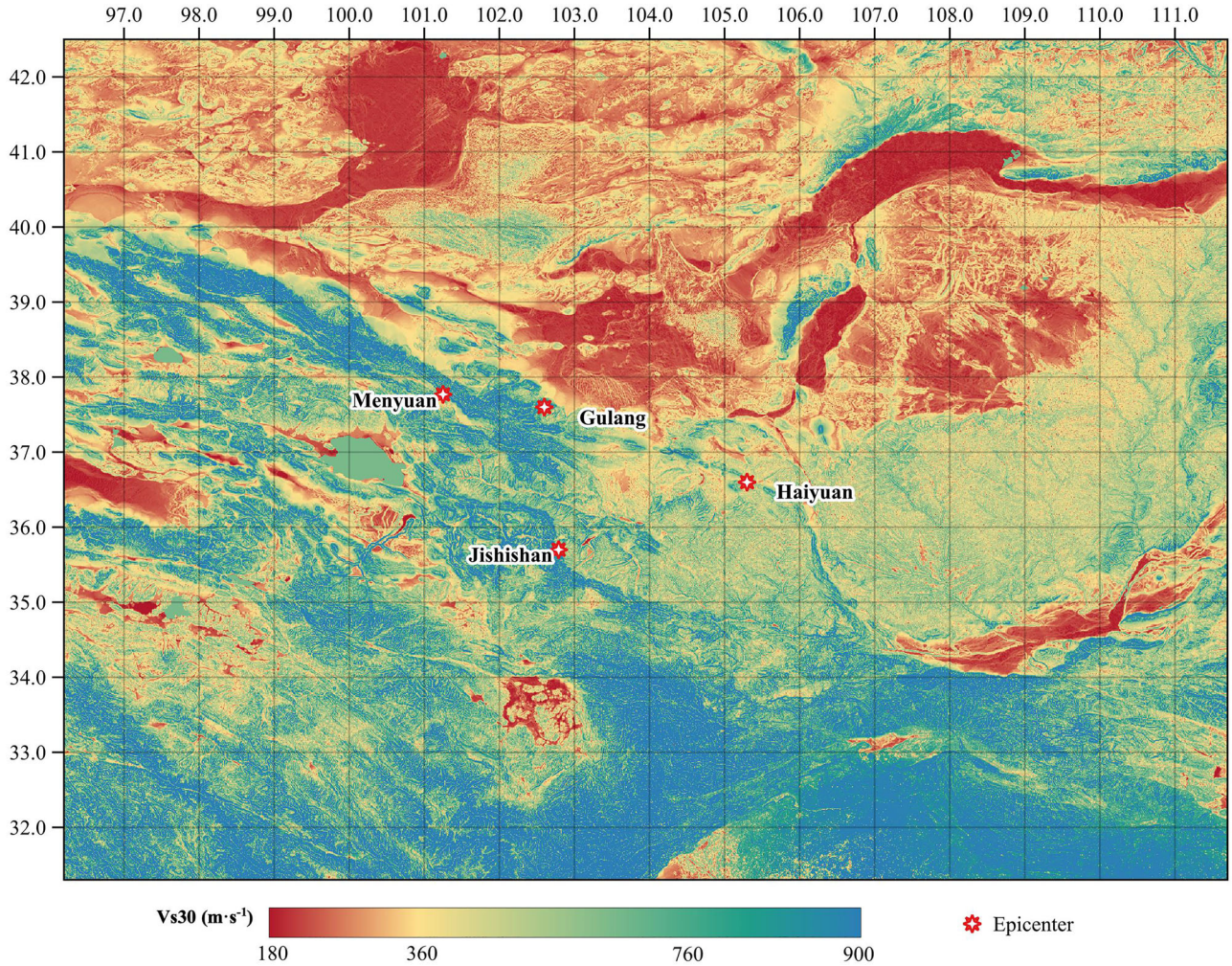

Fig. 5 | Spatial distribution of the average shear-wave velocity in the upper 30 m (Vs30) in the study area.

where PGA_r represents the PGA value corresponding to $V_{s30} = 760$ m s^{-1}. The term f_{hng} represents the hanging-wall effect adopted from the same formulation used in the NGA-West2 model[48]. This term was omitted in the present study ($f_{hng} = 0$) due to insufficient information on the fault geometry for the selected events. The term f_{flt} denotes the fault-type adjustment; $f_{flt} = -0.3742$ for reverse faults with $M_w > 6.5$, and $f_{flt} = 0$ otherwise. Wang[28] model expresses PGA in units of the acceleration due to gravity g, whereas the other models use gal (cm s^{-2}). To ensure consistency and comparability, all predicted and observed PGA values have been converted to m s^{-2} (1 g = 9.8 m s^{-2}, 1 gal = 0.01 m s^{-2}).

In this study, the model domain refers to the spatial evaluation domain used for GMPE calculations. The domain is represented by a regular grid, in which each grid cell corresponds to a 1 × 1 km^2 area, and shares the same spatial extent as the Vs30 dataset shown in Fig. 5, with longitudes ranging from 96.2°E to 111.7°E and latitudes ranging from 31.3°N to 42.5°N. The Vs30 value assigned to each grid cell is directly taken from the corresponding cell of the Vs30 raster. Ground-motion parameters predicted by the GMPEs are evaluated at the center of each grid cell, using the cell-centered Vs30 value and the corresponding source-to-site distance. Consequently, the resulting PGA values represent ground-motion estimates at grid-cell centers within the model domain.

GMPE model evaluation based on residual analysis

We evaluate the performance of the five GMPEs for the Menyuan and Jishishan earthquakes using four evaluation metrics: root mean square error (RMSE), MAE, BIAS, and the coefficient of determination (R^2). The definitions, ideal values, and interpretations of these metrics are summarized in Table 5.

While these metrics provide a straightforward assessment of prediction accuracy, they are not directly used for model ranking. Relying on a single evaluation metric may lead to biased or incomplete conclusions, whereas incorporating multiple metrics raises the challenge of assigning weights in a rational and objective manner. Drawing on the approach of Mak et al.[49] in assessing the applicability of NGA models in Japan and New Zealand, we propose a residual-based method to determine the relative ranking of GMPEs. The calculation is described as follows.

Let us assume that there are M records of strong GMs and N candidate models (in this study, $N = 5$). For the m-th record of the GM, the performance score of model i, denoted as $R_{m,i}$, is calculated as:

$$R_{m,i} = 1 + \sum_{j;j\neq i}^{N} D_{m,ij} \tag{6}$$

$$D_{m,ij} = \begin{cases} 1 \; if \left|P_{m,i} - O_m\right| < \left|P_{m,j} - O_m\right| \\ 0.5 \; if \left|P_{m,i} - O_m\right| = \left|P_{m,j} - O_m\right| \\ 0 \; if \left|P_{m,i} - O_m\right| > \left|P_{m,j} - O_m\right| \end{cases} \tag{7}$$

where $P_{m,i}$ and $P_{m,j}$ are the predictions of models i and j for the m-th record, and O_m is the observed value. That is, model i's prediction is compared against each of the other models based on its absolute deviation from the

Table 5 | Evaluation metrics used for GMPE performance assessment

Index	Formula	Ideal value	Interpretation
RMSE ($m\,s^{-2}$)	$RMSE = \sqrt{\frac{1}{N}\sum_{i=1}^{N}(P_i - O_i)^2}$	0	Measures the standard deviation of prediction errors, sensitive to large errors
MAE ($m\,s^{-2}$)	$MAE = \frac{1}{N}\sum_{i=1}^{N}\lvert P_i - O_i\rvert$	0	Measures average absolute prediction error, more robust to outliers
BIAS ($m\,s^{-2}$)	$BIAS = \frac{1}{N}\sum_{i=1}^{N}(P_i - O_i)$	0	Indicates systematically overestimation or underestimation
R^2	$R^2 = 1 - \frac{\sum_{i=1}^{N}(P_i - O_i)^2}{\sum_{i=1}^{N}(O_i - \bar{O})^2}$	1	Indicates how well predictions explain observed variance

Here, P_i is the predicted value for the ground-motion record i; O_i is the observed value or the ground-motion record i, $\bar{O}$ is the mean of the observed values, N is the total number of observations.

observation. A score of 1 is given if model i's deviation is smaller than that of model j, 0 if worse, and 0.5 if equal. For each record m, the best-performing model will score $R_{m,i} = N$, and the worst will score $R_{m,i} = 1$. The overall performance score R_i of model i is obtained by summing its scores across all M records.

$$R_i = \sum_{m=1}^{M} R_{m,i} \tag{8}$$

GMPE model evaluation based on information-theory

The study adopts an information-theory-based approach proposed by Scherbaum et al.[29] to assess the applicability of candidate GMPEs and to derive appropriate model weights. The Kullback–Leibler divergence, D, is used to quantify the difference between the probability distribution of observed ground motions (which is inherently unknown) and the distribution predicted by a given GMPE model. It is defined as:

$$D(f,g) = E_f\left[\log_2(f)\right] - E_f\left[\log_2(g)\right], \tag{9}$$

where f is the probability distribution of observations, g is the probability distribution related to the selected GMPE, and E_f is the expected value. Scherbaum et al. suggested to calculate $E_f\left[\log_2(g)\right]$ using the average sample log likelihood (LLH)[29]:

$$\mathrm{LLH}(g,x) = -\frac{1}{N}\sum_{i=1}^{N}\log_2\left[g(x_i)\right], \tag{10}$$

where $g(x_i)$ represents the sequence of ground-motion values predicted by a GMPE model, $x = \{x_1, x_2, \ldots x_N\}$ are GM samples obtained from $g(x_i)$. For the sequence x_i (i=1, …, N), the probability density function (PDF) of a normal distribution is determined as:

$$\mathrm{PDF} = \left(\frac{1}{\sqrt{2\pi\sigma}}\right)^N \exp\left(-\sum_{i=1}^{N}\left(\frac{x_i - \mu}{2\sigma^2}\right)^2\right), \tag{11}$$

where μ is the mean (expectation), σ is the standard deviation, and σ^2 is the variance. So, for this PDF, the value of LLH can be estimated as:

$$\mathrm{LLH} = \log_2\left(\sqrt{2\pi}\right) + \log_2\sigma + \frac{\log_2(e)}{2N}\sum_{i=1}^{N}\left(\frac{x_i - \mu}{\sigma}\right)^2. \tag{12}$$

Given the LLH value for each GMPE model g_j, the weight (w_j) and the data support index ($\mathrm{DSI_j}$) can be calculated:

$$w_j = 2^{-\mathrm{LLH}(g_j,x)} \Big/ \sum_{k=1}^{M} 2^{-\mathrm{LLH}(g_k,x)}, \tag{13}$$

$$\mathrm{DSI_j} = 100 \times \frac{w_j - w_{unif}}{w_{unif}}, \text{ where } w_{unif} = \frac{1}{M}, \tag{14}$$

where w_{unif} is the uniform weight, and $M = 5$ in this study. The GM $\{x_i\}$ are sampled from GMPEs for all grid cells of the model domain within a circular region of specified radius centered at the epicenter. Based on the obtained $\{x_i\}$, the LLH, w_j and DSI_j for each model were calculated following the procedure described above (Eqs. 9–14). Only the GMPEs with positive DSI values were considered applicable, and their corresponding weights (w_i) and rankings were subsequently determined.

Within this framework, LLH is not used as a standalone ranking metric but as an input to derive DSI and normalized model weights, which underpin the final model ranking reported in this study. Consequently, LLH, DSI, and the resulting weights are interpreted in a relative sense by comparing candidate GMPEs within the same model set, study region, and evaluation procedure, rather than as absolute measures of predictive performance.

Data availability

The observational strong-motion dataset used in this study was obtained from the China Earthquake Administration data portal (https://data.earthquake.cn/datashare/report.shtml?PAGEID=ground_motion_list). The Vs30 data are taken from the USGS global Vs30 model (https://earthquake.usgs.gov/data/vs30). The ground-motion prediction datasets generated by the evaluated GMPEs have been archived on GitHub and are available at https://github.com/EdenYYT/RapidGMPE/tree/Data.

Code availability

The information-theoretic GMPE evaluation code developed in this study is openly available on GitHub at https://github.com/EdenYYT/RapidGMPE. A graphical user interface (GUI) version of the software has also been implemented and is provided for practical use. Additional scripts used in the analyses are available from the authors upon reasonable request.

Received: 23 December 2025; Accepted: 26 February 2026;
Published online: 13 March 2026

References

1. Molnar, P. & Tapponnier, P. Cenozoic tectonics of Asia: effects of a continental collision. *Science* **189**, 419–426 (1975).
2. Tapponnier, P. et al. Oblique stepwise rise and growth of the Tibet Plateau. *Science* **294**, 1671–1677 (2001).
3. Zhang, P. et al. Active tectonic blocks and strong earthquakes in the continent of China. *Sci. China Ser. Earth Sci.* **46**, 13–24 (2003).
4. Deng, Q., Cheng, S., Ma, J. & Du, P. Seismic activities and earthquake potential in the Tibetan Plateau. *Chin. J. Geophys.* **57**, 2025–2042 (2014).
5. Li, H. et al. Continental tectonic deformation and seismic activity: a case study from the Tibetan Plateau. *Acta Geol. Sin.* **95**, 194–213 (2021).
6. Zheng, D. et al. Progressive northward growth of the northern Qilian Shan–Hexi Corridor (northeastern Tibet) during the Cenozoic. *Lithosphere* **9**, 408–416 (2017).
7. Shao, R., Shen, X. & Zhanag, Y. Crustal anisotropy and tectonic implications beneath southeastern Gansu province in northeastern margin of the Tibetan Plateau. *Chin. J. Geophys.* **62**, 3340–3353 (2019).
8. Gao, G. et al. Gravity anomalies and deep structure of the northeastern Tibetan Plateau and adjacent areas. *J. Asian Earth Sci.* **278**, 106430 (2025).
9. Lasserre, C. et al. Postglacial left slip rate and past occurrence of M≥8 earthquakes on the Western Haiyuan Fault, Gansu, China. *J. Geophys. Res. Solid Earth* **104**, 17633–17651 (1999).
10. Zhang, P. et al. Discussion on late cenozoic growth and rise of Northeastern Margin of the Tibetan Plateau. *Quat. Sci.* **26**, 5–13 (2006).
11. Gao, R. et al. Tectonic development of the northeastern Tibetan Plateau as constrained by high-resolution deep seismic-reflection data. *Lithosphere* **5**, 555–574 (2013).
12. Fu, Y. & Xiao, Z. Ambient noise tomography of Rayleigh and Love wave in Northeast Tibetan plateau and adjacent regions. *Chin. J. Geophys.* **63**, 860–870 (2020).
13. Xin, Z. et al. Electrical structure of the eastern segment of the Qilian orogenic belt revealed by 3-D inversion of magnetotelluric data: new insights into the evolution of the northeastern margin of the Qinghai-Tibet Plateau. *J. Asian Earth Sci.* **210**, 104707 (2021).
14. Li, S., Guo, Z., Yu, Y., Wu, X. & Chen, Y. J. Imaging the Northeastern Crustal Boundary of the Tibetan Plateau With Radial Anisotropy. *Geophys. Res. Lett.* **49**, e2022GL100672 (2022).
15. Dai, Y. et al. Decoupled anisotropy in the lower crust and upper mantle extracted by the Wave Gradiometry method resolves the differential deformation mechanisms beneath the northeastern Tibetan Plateau. *Earth Planet. Sci. Lett.* **633**, 118654 (2024).
16. Ren, P., Guo, Z., Liu, Y., Luo, B. & Wu, X. Seismic evidence of basin development in NE tibetan plateau in response to deep crustal dynamics from joint inversion of rayleigh wave ellipticity and phase velocity. *Geophys. Res. Lett.* **51**, e2024GL108589 (2024).
17. Han, L. et al. Coseismic slip gradient at the western terminus of the 1920 Haiyuan Mw 7.9 earthquake. *J. Struct. Geol.* **152**, 104442 (2021).
18. Xu, X., Wu, X., Yu, G., Tan, X. & Li, K. Seismo-geological signatures for identifying M≥7. 0 earthquake risk areas and their premilimary application in Mainland China. *Seismol. Geol.* **39**, 219–275 (2017).
19. Wang, S., Xu, K. & Zhang, M. Past century stress evolution and seismic hazards in the Haiyuan Fault in northeastern Tibetan Plateau: a case of the 2022 Menyuan *M*S6.9 earthquake. *Adv. Space Res.* **75**, 8411–8424 (2025).
20. Douglas, J. Earthquake ground motion estimation using strong-motion records: a review of equations for the estimation of peak ground acceleration and response spectral ordinates. *Earth Sci. Rev.* **61**, 43–104 (2003).
21. Boore, D. M. & Atkinson, G. M. Ground-motion prediction equations for the average horizontal component of PGA, PGV, and 5%-damped PSA at spectral periods between 0.01 s and 10.0 s. *Earthq. Spectra* **24**, 99–138 (2008).
22. Wang, D., Xie, L., Abrahamson, N. A. & Li, S. Comparison of Strong Ground Motion from the Wenchuan, China, Earthquake of 12 May 2008 with the Next Generation Attenuation (NGA) Ground-Motion Models. *Bull. Seismol. Soc. Am.* **100**, 2381–2395 (2010).
23. Ji, K., Wen, R., Ren, Y., Wang, H. & Huang, X. Applicability of the NGA model in Lushan earthquake region. *Chin. J. Rock Mech. Eng.* **35**, 2990–2999 (2016).
24. Bai, Y. Comparison of strong ground motion recordings of the Lushan, China, Earthquake of 20 April 2013 with the next generation attenuation (NGA)-West2 ground-motion models. *Bull. Seismol. Soc. Am.* **107**, 1724–1736 (2017).
25. Douglas, J. *Ground Motion Prediction Equations 1964-2021* http://www.gmpe.org.uk (2022).
26. Naveen, Sharma, M. L. & Mittal, H. Advancing earthquake hazard mitigation: Ground motion prediction for the Himalayan region. *Soil Dyn. Earthq. Eng*. **202**, 110001 (2026).
27. Yu, Y., Li, S. & Xiao, L. Development of ground motion attenuation relations for the new seismic hazard map of China. *Technol. Earthq. Disaster Prev.* **8**, 24–33 (2013).
28. Wang, S. et al. Ground motion attenuation model in the northeast margin of Qinghai-Tibet Plateau region and its application in the evaluation of seismic impact field. *J. Xian Univ. Archit. Technol. Sci. Ed.* **55**, 301–309 (2023).
29. Scherbaum, F., Delavaud, E. & Riggelsen, C. Model selection in seismic hazard analysis: an information-theoretic perspective. *Bull. Seismol. Soc. Am.* **99**, 3234–3247 (2009).
30. Delavaud, E., Scherbaum, F., Kuehn, N. & Allen, T. Testing the global applicability of ground-motion prediction equations for active shallow crustal regions. *Bull. Seismol. Soc. Am.* **102**, 707–721 (2012).
31. Baro, O., Kumar, A. & Ismail-Zadeh, A. Seismic hazard assessment of the Shillong Plateau, India. *Geomat. Nat. Hazards Risk* **9**, 841–861 (2018).
32. Hu, J. & Sun, J. Analysis of the typical ground-motion attenuation relationships in China based on information-theory. *World Earthq. Eng* **34**, 65–70 (2018).
33. Huo, J. & Hu, Y. Study on attenuation laws of ground motion parameters. *Earthq. Eng. Eng. Dyn.* **12**, 1–11 (1992).
34. SI, H. & Midorikawa, S. New attenuation relationships for peak ground acceleration and velocity considering effects of fault type and site condition. *J. Struct. Constr. Eng. Trans. AIJ* **64**, 63–70 (1999).
35. Standardization Administration of the People's Republic of China. Seismic ground motion parameters zonation map of China (2015).
36. Zhou, D. *An Analysis on the Suitabiiity of Several GMPEs in Western China* (Institute of Geophysics, China Earthquake Administration, 2019).
37. Han, G., Dai, D., Li, Y., Xi, N. & Sun, L. Rapid report of the December 18, 2023 MS 6.2 Jishishan earthquake, Gansu, China. *Earthq. Res. Adv.* **4**, 100287 (2024).
38. Allmann, B. P. & Shearer, P. M. Global variations of stress drop for moderate to large earthquakes. *J. Geophys. Res. Solid Earth* **114**, (2009).
39. Liu, Z. et al. Source parameters and slip distribution of the 2023 Mw 6.0 Jishishan (Gansu, China) Earthquake Constrained by InSAR Observations. *Geomat. Inf. Sci. Wuhan Univ.* **50**, 344–355 (2025).
40. Liu, Y., Xi, N., Dai, D., Zhi, M. & Cai, J. DataSet of strong ground motion parameters of magnitude M4.0 and above earthquakes in China since 2020. https://doi.org/10.12080/nedc.11.ds.2024.0002 (2024).
41. Su, R. et al. Surface rupture and damage characteristics of the 2023 MS6.2 Jishishan earthquake, Gansu. *Chin. J. Geophys.* **67**, 3454–3471 (2024).
42. Huo, J., Hu, Y. & Feng, Q. Study on estimation of ground motion from seismic intensity. *Earthq. Eng. Eng. Vib.* **12**, 1–15 (1992).
43. Su, Y., Ma, W., Ma, E. & Wu, Z. Seismic hazard comparative analysis and zonation along Qinghai—Tibet Engineering Corridor. *China Earthq. Eng. J.* **39**, 311–320 (2017).
44. Yu, Y. & Wang, S. Attenuation relations for horizontal peak ground acceleration and response spectrum in northeastern Tibetan Plateau region. *Acta Seismol. Sin. Engl. Ed.* **17**, 651–661 (2004).

45. Chen, W., Wang, D., Si, H. & Zhang, C. Rapid estimation of seismic intensities using a new algorithm that incorporates array technologies and ground-motion prediction equations (GMPEs). *Bull. Seismol. Soc. Am.* **112**, 1647–1661 (2022).
46. Zhang, C., Chen, W., Si, H. & Zhao, H. Intensity rapid evaluation of Maduo M7.4 earthquake in Qinghai Province, 2021. *China Earthq. Eng.* **43**, 876–882 (2021).
47. Ma, X. et al. Scenario construction of urban buildings and earthquake risk assessment: an example of Maqu County. *Earthq. Eng. Eng. Dyn.* **43**, 46–55 (2023).
48. Campbell, K. W. & Bozorgnia, Y. *NGA-West2 Campbell-Bozorgnia Ground Motion Model for the Horizontal Components of PGA, PGV, and 5%-Damped Elastic Pseudo-Acceleration Response Spectra for Periods Ranging from 0.01 to 10 Sec*. https://peer.berkeley.edu/sites/default/files/webpeer-2013-06-kenneth_w._campbell_and_yousef_bozorgnia.pdf (2013).
49. Mak, S., Cotton, F., Gerstenberger, M. & Schorlemmer, D. An evaluation of the applicability of NGA-West2 ground-motion models for Japan and New Zealand. *Bull. Seismol. Soc. Am.* **108**, 836–856 (2018).

Acknowledgements

This research was supported by the China Scholarship Council and the National Key R&D Program of China (Grant No. 2022YFC3004404).

Author contributions

A.I. conceived the idea of this research. Y.Y. contributed to data validation and quantitative analysis as well as to discussion and interpretation of the results (together with A.I.); wrote the manuscript and prepared figures. A.I. and J.W. reviewed and edited the manuscript.

Funding

Open Access funding enabled and organized by Projekt DEAL.

Competing interests

Author Alik Ismail Zadeh is an Editorial Board Member of npj Natural Hazards. Alik Ismail Zadeh was not involved in the journal's review of, or decisions related to, this manuscript. The other authors declare no competing financial or non-financial interests.

Additional information

Supplementary information The online version contains supplementary material available at https://doi.org/10.1038/s44304-026-00196-6.

Correspondence and requests for materials should be addressed to Youtian Yang.